

Local rheology relation with variable yield stress ratio across dry, wet, dense, and dilute granular flows

Thomas Pähtz^{1,2,*}, Orencio Durán³, David N. de Klerk^{4,5}, Indresan Govender⁶, and Martin Trulsson⁷

1. Institute of Port, Coastal and Offshore Engineering,
Ocean College, Zhejiang University, 310058 Hangzhou, China

2. State Key Laboratory of Satellite Ocean Environment Dynamics,
Second Institute of Oceanography, 310012 Hangzhou, China

3. Department of Ocean Engineering, Texas A&M University, College Station, Texas 77843-3136, USA

4. Centre for Minerals Research, University of Cape Town, Private Bag Rondebosch, 7701, South Africa

5. Department of Physics, University of Cape Town, Private Bag Rondebosch, 7701, South Africa

6. School of Engineering, University of KwaZulu-Natal, Glenwood, 4041, South Africa

7. Theoretical Chemistry, Department of Chemistry, Lund University, Lund, Sweden

Dry, wet, dense, and dilute granular flows have been previously considered fundamentally different and thus described by distinct, and in many cases incompatible, rheologies. We carry out extensive simulations of granular flows, including wet and dry conditions, various geometries and driving mechanisms (boundary-driven, fluid-driven, and gravity-driven). For all simulated conditions, except for fluid-driven and gravity-driven flows close to the flow threshold, we find that the Mohr-Coulomb friction coefficient μ scales with the square root of the local Péclet number Pe , provided that the particle diameter exceeds the particle mean free path. With decreasing Pe and granular temperature gradient M , this general scaling breaks down as the system becomes increasingly isotropic, allowing the mechanical stabilization of the flow. This leads to a yield condition with a variable yield stress ratio characterized by M .

Reliable large-scale simulations and thus predictions of geophysical and industrial processes require a deep understanding of the continuum properties of granular flows (i.e., the collective motion of granular particles). However, existing theories of the granular flow continuum (the “rheology”) are limited to small subsets of the physical conditions under which such processes can occur. For example, although geophysical granular flows are often wet (i.e., significantly affected or driven by ambient fluid) [1–3] and consist of coexisting dense (liquid-like) and dilute (gas-like) flow layers [3–6], even understanding comparably simple dry, dense-only or dilute-only flows has remained a major challenge [7–9].

Existing rheologies for non-cohesive and non-quasistatic flows of sufficiently hard granular particles can be classified in terms of the particle volume fraction ϕ (the fraction of space covered by particles), particle-fluid-density ratio $s \equiv \rho_p/\rho_f$, and Stokes number $St \equiv \rho_p \dot{\gamma} d^2/\eta_f$, where d is the particle diameter, $\dot{\gamma}$ the granular shear rate, and η_f the fluid viscosity. Dilute, dry flows ($\phi \lesssim 0.5$, $s \rightarrow \infty$, $St \rightarrow \infty$) have been described by the kinetic theory of dry granular gases [9]; dense, dry flows ($\phi \gtrsim 0.5$, $s \rightarrow \infty$, $St \rightarrow \infty$) by the local viscoplastic rheology [10] and its nonlocal extensions [11–14]; dense solid-liquid suspensions ($\phi \gtrsim 0.5$, $s \simeq 1$, variable St) by different (partially incompatible [15]) visco-inertial rheologies [16–21]; and sediment transport driven by liquids (variable ϕ , $1 < s < 3$, variable St) by modified viscoplastic or visco-inertial rheologies [22–24]. Furthermore, different rather complex and controversial approaches exist to extend kinetic theory to solid-gas suspensions [25–27] or the dense regime [28–30].

Here we show that, despite their fundamental dif-

ferences, granular flows from the entire phase space (ϕ, s, St) actually obey a common scaling law for the Mohr-Coulomb friction coefficient μ , the knowledge of which is essential for any rheological description.

We carry out discrete element method-based simulations of granular flows for a variety of geometries and driving mechanisms (Table I and Fig. 1), which cover the entire phase space: (i) two-dimensional sediment transport driven by a large variety of Newtonian fluids, (ii) rapid gravity-driven flows in ambient static air of varying viscosity, (iii) two-dimensional uniformly sheared viscous suspensions in density-matched fluid of varying viscosity, (iv) two-dimensional dry uniform shear flows, (v) three-dimensional rotating drum flows lubricated by a density-matched fluid, and (vi) a three-dimensional dry rotating drum flow. In all simulations, contacting particles interact via normal repulsion (restitution coefficient e , modeled through viscous damping), governed either by a linear or Hertzian law, and tangential friction (contact friction coefficient μ_c , Table I). Details are described below.

Flow geometry	Driven by	Contact model (e, μ_c)
Sediment transport (2D)	Fluid	Linear (0.9, 0.5)
Rapid gravity flows (2D)	Gravity	Linear (0.9, 0.5)
Sheared suspensions (2D)	Boundary	Linear (0.1, 0.4)
Dry shear flows (2D)	Boundary	Linear (0.1, 0.4)
Lubricated drum flows (3D)	Boundary	Hertz (0.5, 0.5)
Dry drum flow (3D)	Boundary	Hertz (0.5, 0.5)

TABLE I. Summary of simulated granular flows.

Sediment transport and gravity flows.—The numerical

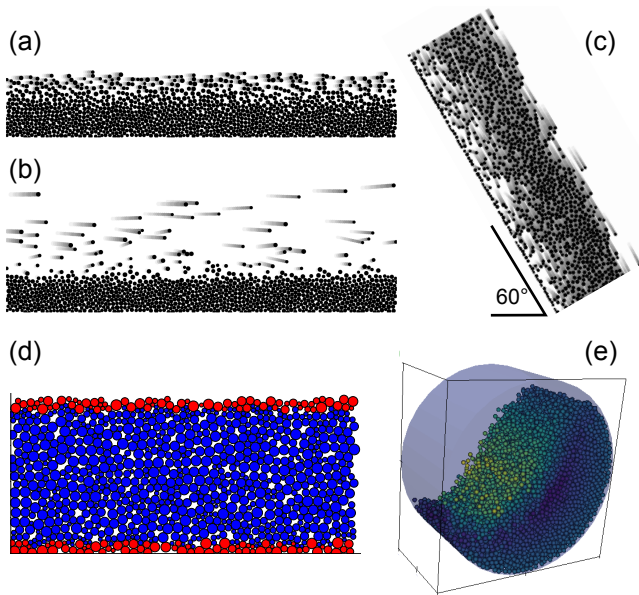


FIG. 1. Visualizations of numerical simulations of (a & b) sediment transport driven by various Newtonian fluids, (c) rapid gravity-driven flows in ambient static air, (d) uniformly sheared flows, and (e) rotating drum flows.

model couples a discrete element method for the particle motion (stiffness $k = 5000mg/d$) under gravity, buoyancy, and fluid drag with a continuum Reynolds-averaged description of hydrodynamics (described in detail and/or validated in Refs. [31–35]). Spherical particles ($\sim 10^4$) with mild polydispersity are confined in a quasi-two-dimensional, vertically infinite domain of length $\sim 10^3d$ with periodic boundary conditions in the flow direction. The bottom-most particle layer is more dissipative and glued on a bottom wall. The Reynolds-Averaged Navier-Stokes equations are combined with an improved mixing length approximation, which can be used to calculate the mean turbulent fluid velocity at high particle concentrations. For gravity flows, the ambient fluid is kept static.

Simulations are carried out for varying density ratio s , Galileo number $\text{Ga} \equiv \rho_f \sqrt{(s-1)gd^3}/\eta_f$, Shields number $\Theta \equiv \tau_f/[(\rho_p - \rho_f)gd]$, and inclination angle α , where g is the gravitational constant and τ_f is the bed fluid shear stress. For gravity flows, we simulate conditions with $s = 2000$, $\text{Ga} \in [2, 100]$, $\Theta = 0$, and α between the flow threshold and 60° . For sediment transport, we simulate conditions with $s \in [2.65, 2000]$, $\text{Ga} \in [0.1, 100]$, $\alpha = 0$, and Θ above the flow threshold, which correspond to five different transport regimes (Table II) [34]. Following the symmetry along the flow direction, simulation data are averaged over horizontal layers of variable thickness depending on the particle volume fraction [31].

Uniformly sheared particle and suspension flows.—The numerical model couples a discrete element method for the particle motion ($k = 2000P_{yy}d$) under viscous fluid

Sediment transport regime	Condition
Viscous bedload transport	$\sqrt{s}\text{Ga} < 20$
Turbulent bedload transport	$\sqrt{s}\text{Ga} \geq 20 \wedge s < 10$
Bedload-saltation transition	$20 \leq \sqrt{s}\text{Ga} < 80 \wedge s \geq 10$
Viscous saltation transport	$\sqrt{s}\text{Ga} \geq 80 \wedge s \geq 10 \wedge \sqrt[4]{s}\text{Ga} < 32$
Turbulent saltation transport	$\sqrt{s}\text{Ga} \geq 80 \wedge s \geq 10 \wedge \sqrt[4]{s}\text{Ga} \geq 32$

TABLE II. Sediment transport regimes [34].

drag and torque, with the Stokes equations for laminar flow (described in detail in Refs. [17, 36]). Two-dimensional disks ($\sim 10^3$) with moderate polydispersity are confined within a shear cell composed by two rough walls, created by gluing together two dense layers of grains, with periodic boundary conditions along the flow direction parallel to the walls. The position of the walls is controlled to ensure constant confining pressure P_{yy} and mean shear rate.

Simulations are carried out for varying volume fraction (in the range $\phi > 0.24$, where ϕ is calculated as $2/3$ of the disk area fraction, like for spheres confined in two dimensions) and two general cases: no ambient fluid (dry condition) and an ambient density-matched liquid with varying dimensionless viscosity ($s = 1$, $\eta_f/\sqrt{\rho_f P_{yy}d^2} = [10^{-3}, 10^{-2}, 10^{-1}, 10^0, \infty]$). Simulation data are averaged over the entire shear cell.

Rotating drum flows.—The numerical model uses a discrete element method for the particle motion ($k = 17000mg/d^{3/2}$) under lubrication forces [18] and gravity. The contact model employs the LIGGGHTS implementation of Hertzian contacts, which ensures a value of e [37, 38]. Spherical monodisperse particles ($\sim 10^4$) are confined within a closed horizontal cylinder (drum) of radius $20d$ and width $20d$ rotating at a constant rate ω .

Simulations are carried out for no ambient fluid (dry condition) and an ambient density-matched liquid with varying dimensionless viscosity ($s = 1$, $\eta_f/(\rho_f\omega d^2) = [1/160, 1/16, 3/16]$). Simulation data are averaged using an anisotropic Gaussian smoothing function of dimension $3d \times 3d \times 20d$.

General rheology relation.—Contact (\mathbf{P}^c) and kinetic (\mathbf{P}^k) granular stresses are calculated from the simulation data using the method given in Ref. [39], which ensures that the granular temperature $T = \sum_i P_{ii}^k/(\rho_p\phi D)$ (the root-mean-square of the particle fluctuation velocity), where D is the number of space dimensions, is insensitive to the coarse-graining width. Furthermore, the shear rate $\dot{\gamma}$ is calculated as the norm of the deviatoric component of the strain rate tensor $\epsilon_{ij} \equiv \partial_i\langle v_j \rangle + \partial_j\langle v_i \rangle$, which reads $\dot{\gamma} \equiv \|\epsilon^d\| = \sqrt{\sum_{ij} \epsilon_{ij}^d \epsilon_{ij}^d/2}$, where $\epsilon_{ij}^d = \epsilon_{ij} - \sum_k \epsilon_{kk} \delta_{ij}/D$. Finally, we calculate the Mohr-Coulomb friction coefficient $\mu \equiv \max_{i,j} |P_i - P_j|/|P_i + P_j|$ from the principal components P_i of the granular stress

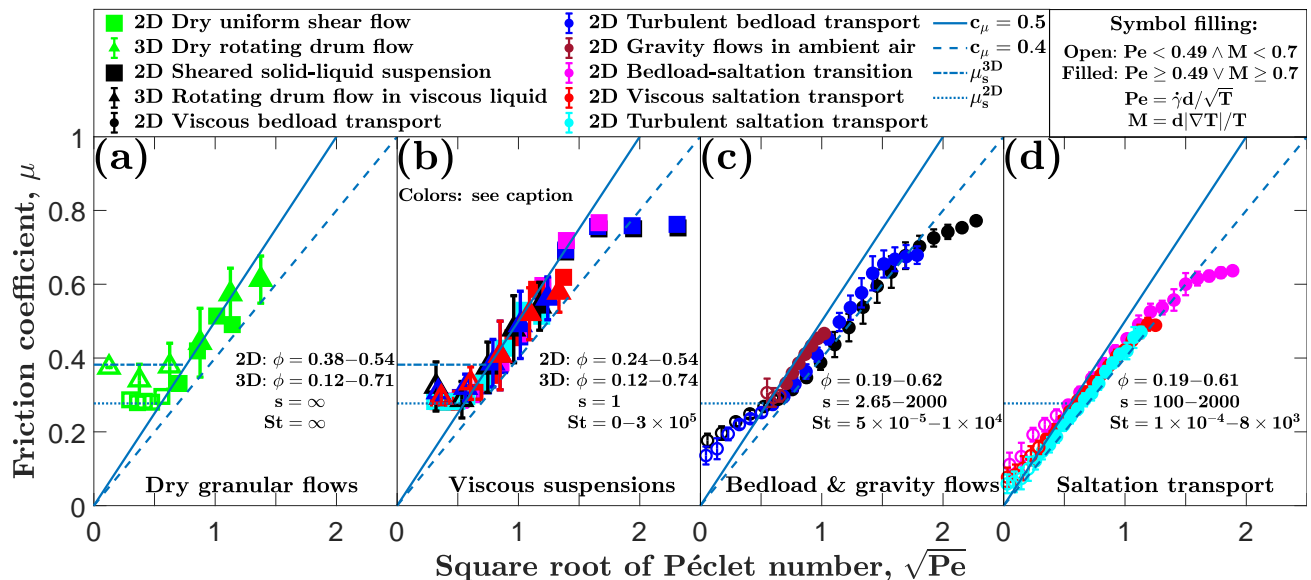


FIG. 2. Mohr-Coulomb friction coefficient μ vs square root of Péclet number ($\sqrt{\text{Pe}}$) for data from discrete element method-based simulations of (a) dry granular flows, (b) viscous suspensions in density-matched liquids, (c) bedload transport and gravity flows, and (d) saltation transport. For the rotating drum flows in (a) and (b) and the sediment transport and gravity flow simulations in (c) and (d), Pe and μ depend on the location within the flow. The value of μ at each location with $\lambda(\phi) < d$ and either $\sqrt{\text{Pe}} < 0.7 \wedge M < 0.7$ (open symbols) or $\sqrt{\text{Pe}} \geq 0.7 \vee M \geq 0.7$ (filled symbols) is allocated to the corresponding bin of $\sqrt{\text{Pe}}$. Each bin in (a) and (b) consists of data from a single rotating drum simulation, whereas each bin in (c) and (d) consists of data from various simulations of the same regime (Table II). The mean and standard deviation of μ within each bin are represented by the symbols and their error bars, respectively. For the squares in (b), the color order (cyan, red, magenta, blue, black) corresponds to $\eta_f/\sqrt{\rho_f P_{yy} d^2} = [10^{-3}, 10^{-2}, 10^{-1}, 10^0, \infty]$. For the triangles in (b), the color order (red, blue, black) corresponds to $\eta_f/(\rho_f \omega d^2) = [1/160, 1/16, 3/16]$.

tensor $\mathbf{P} = \mathbf{P}^c + \mathbf{P}^k$ (a Drucker-Prager definition of μ yields slightly but statistically significantly worse results for our three-dimensional flows).

For both dilute and dense flow conditions (defined shortly), we find that the friction coefficient μ is only a function of the Péclet number $\text{Pe} \equiv \dot{\gamma}d/\sqrt{T}$ [28] and scales as

$$\mu = c_\mu \sqrt{\text{Pe}}, \quad (1)$$

almost everywhere within all simulated conditions (Fig. 2, filled symbols), except for sediment transport and gravity flows too close to the flow threshold (which are excluded from Figs. 2c and 2d) because of nonlocal effects (see supplementary materials for details [40]). The scale parameter c_μ slightly depends on the driving conditions, with the smallest value found for viscous bedload transport. For uniformly sheared flows, c_μ varies significantly with the contact friction coefficient ($c_\mu \simeq 0.3$ for $\mu_c = 0$, $c_\mu \simeq 0.55$ for $\mu_c = 100$) but not with the normal restitution coefficient e , even in the extreme cases $\mu_c = 100$ (no sliding) and $\mu_c = 0$ (always sliding) [40]. This suggests that Eq. (1) originates from a competition between macroscopic shearing (rate $\dot{\gamma}$) and thermal diffusion perpendicular to the shearing motion (rate $\propto \sqrt{T}/d$) because a particle diffusing from a shear layer into a hole

of an adjacent shear layer experiences mainly tangential contacts rather than normal contacts. Note that this diffusion interpretation is similar to the interpretation of the inertial number, viscous number, and wet inertial number as the ratios between rearrangement and shearing time scales [41].

We define dilute and dense conditions – as opposed to rarefied ones – in terms of the mean free path λ through the condition $\lambda < d$, where $\lambda(\phi) = \sqrt{2}d/(12\phi)$ for spherical particles and $\lambda(\phi) = \pi d/(12\sqrt{2}\phi)$ for spheres confined in two dimensions. In fact, we hypothesize that at least some of the few deviations from the scaling $\mu \propto \sqrt{\text{Pe}}$ at large Pe (Fig. 2) are related to a transition from dilute to rarefied flows at large shear rates, where kinetic stresses are dominant and thus μ limited by the geometrical constraints of high energy collisions [35]. Note that conditions with small overall dissipation (e.g., shearing flows with small viscosity and $e = 0.9$) deviate at smaller Pe [40].

Variable yield stress ratio.—Interestingly, deviations from the scaling in Eq. (1) at small Pe (larger-than-predicted values of μ) are well characterized by the dimensionless granular temperature gradient $M \equiv d|\nabla T|/T$ and seem to occur whenever $M \lesssim 0.7$ and $\text{Pe} \lesssim 0.5$ (Fig. 2, open symbols). For shear rate

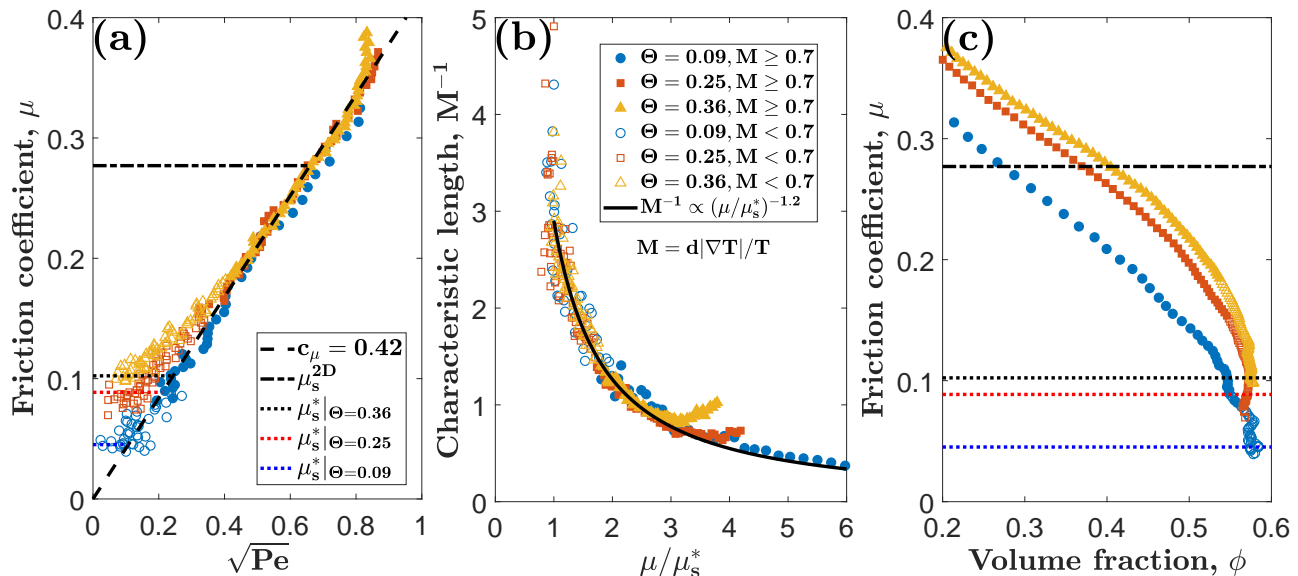


FIG. 3. (a) Mohr-Coulomb friction coefficient μ vs square root of Péclet number ($\sqrt{\text{Pe}}$). (b) Characteristic length M^{-1} vs rescaled friction coefficient μ/μ_s^* . (c) μ vs particle volume fraction ϕ . Symbols correspond to data with $\lambda(\phi) < d$ from simulations of turbulent saltation transport ($s = 2000$, $\text{Ga} = 5$) for three different Shields numbers Θ .

and pressure-controlled homogeneous flows (e.g., uniform shear, squares in Figs. 2a and 2b), where temperature gradients are negligible ($M \sim 0$), these deviations are owed to the fact that μ converges to the yield stress ratio μ_s ($\mu_s^{2\text{D}} = 0.277$ [17], $\mu_s^{3\text{D}} = 0.382$ [28]) in the limit of vanishing shear rate. From Eq. (1), we find that this yield transition in homogeneous flows starts at $\text{Pe} = (\mu_s/c_\mu)^2 \approx 0.5$.

For inhomogeneous flows, like sediment transport (Figs. 2c, 2d, and 3a), the friction coefficient μ can be substantially smaller than μ_s when $\text{Pe} \lesssim 0.5$, at which point deviations from the scaling in Eq. (1) are controlled by temperature gradients, in particular the condition $M \lesssim 0.7$. These deviations have several elements in common with a yield transition, as illustrated in Fig. 3 for turbulent saltation transport. First, μ seems to converge to a finite value μ_s^* in the limit of vanishing shear rate (Fig. 3a). Second, the dimensionless characteristic length M^{-1} , associated with spatial changes in the granular temperature, collapses as a function of μ/μ_s^* with a peak at $\mu/\mu_s^* = 1$ (Fig. 3b). This peak is reminiscent of the divergence of the relaxation length associated with spatial changes of the shear rate ($\dot{\gamma}$) and granular stresses (P_{ij}) when approaching the yield condition ($\mu \rightarrow \mu_s$) in existing nonlocal rheology models [13] (an in-depth comparison between the various forms of nonlocality will be carried out in the future). Finally, ϕ approaches the packing fraction as $\mu \rightarrow \mu_s^*$ (Fig. 3c). We thus conclude that μ_s^* is the analogue of μ_s for inhomogeneous flows with sufficiently large temperature gradients.

The onset of the yield transition is thus a func-

tion of the dimensionless temperature gradient M and Péclet number Pe , as they both characterize the level of anisotropy in the system. At low M and Pe , the flow is more isotropic and can therefore be mechanically stabilized [42]. However, for sediment transport, even at low Pe (i.e., when thermal diffusion dominates), the relatively large temperature gradient induced by the transport layer prevents the yield transition and μ continues to obey Eq. (1). Note that, for inhomogeneous flows, general local relationships, like Eq. (1), are not expected to work at locations that exhibit a sub-critical stress ratio ($\mu < \mu_s$) [13].

Relation to viscoplastic rheology and its nonlocal extensions.—For a dry granular flow, Navier-Stokes order granular kinetic theories, and their extensions to the dense regime, express the rescaled granular viscosity and pressure, $\|\boldsymbol{\tau}\|/(\rho_p d \sqrt{T} \dot{\gamma})$ and $P/(\rho_p T)$ (where $P = \sum_i P_{ii}/D$), as functions of the particle volume fraction ϕ provided that the shear stress tensor $\boldsymbol{\tau} = P\mathbf{I} - \mathbf{P}$ and deviatoric strain rate tensor $\boldsymbol{\epsilon}^d$ are aligned [9, 28–30]. When combined with Eq. (1), these lead to the prediction that μ is only a function of ϕ or, equivalently, of the inertial number $I \equiv \dot{\gamma}d/\sqrt{P/\rho_p}$. That is, the viscoplastic $\mu(I)$ rheology [10], which assumes alignment between $\boldsymbol{\tau}$ and $\boldsymbol{\epsilon}^d$, is recovered in Navier-Stokes order. Furthermore, the prediction that the rescaled granular fluidity $f \equiv \dot{\gamma}d/(\mu\sqrt{T}) = \text{Pe}/\mu$, which plays a crucial role in non-local extensions of the $\mu(I)$ rheology [13], solely depends on ϕ [14] is also recovered from Eq. (1) in Navier-Stokes order. However, we find that the predicted relation $\mu(\phi)$, and thus $\mu(I)$ and $f(\phi)$, fails to describe turbulent salta-

tion transport (Fig. 3c) despite the fact that these conditions are essentially dry for $\mu > \mu_s^*$ because of a large density ratio $s = 2000$, large Stokes number [$St \in (10, 300)$], and particles that are usually much slower than the terminal settling velocity. Hence, kinetic theories beyond the Navier-Stokes order (e.g., [43–45]) may be needed to describe sediment transport. Note that the previously reported misalignment between τ and ϵ^d in rotating drum flows [46] is also associated with a breakdown of standard kinetic theory (a paper on this issue is in preparation).

Conclusions.—In this study, we have shown that, under certain relatively weak constraints, the Mohr-Coulomb friction coefficient μ obeys the general scaling $\mu = c_\mu \sqrt{\text{Pe}}$, with the Péclet number defined as $\text{Pe} = \dot{\gamma}d/\sqrt{T}$. The scaling parameter c_μ varies with the tangential friction coefficient μ_c but not with the normal coefficient of restitution e (extended granular kinetic theory predicts the exact opposite [28, 30]), from which we have inferred that this scaling likely originates from a competition between macroscopic shearing (rate $\dot{\gamma}$) and thermal diffusion perpendicular to the shearing motion (rate $\propto \sqrt{T}/d$).

The yield stress ratio of granular media, below which granular flows either stop or fundamentally change [13], is currently thought to be independent of the flow geometry [42]. However, for sediment transport the scaling $\mu \propto \sqrt{\text{Pe}}$ even holds for friction coefficients as low as $\mu \simeq 0.08$ and is accompanied by a very low yield stress ratio ($\mu_s^* \simeq 0.04$ despite of frictional particles) caused by relatively large values of the dimensionless temperature gradient $M \equiv d|\nabla T|/T$, which prevent the mechanical stabilization of the flow. Future studies should investigate this link between μ_s^* and T because it may play a role in explaining long-standing open problems, such as the reduction of friction in long-runout landslides [47–49].

Thomas Pähtz acknowledges support from grant National Natural Science Foundation of China (No. 11750410687). Martin Trulsson acknowledges funding from the Swedish Research Council (621-2014-4387). Simulations of rotating drums were performed using facilities provided by the University of Cape Town’s ICTS High-Performance Computing team (<http://hpc.uct.ac.za>). The uniformly DEM simulations were performed on resources provided by the Swedish National Infrastructure for Computing (SNIC) at the centre for scientific and technical computing at Lund University (LUNARC).

* 0012136@zju.edu.cn

[1] S. Courrech du Pont, P. Gondret, B. Perrin, and M. Rabaud, “Granular avalanches in fluids,” *Physical Review Letters* **90**, 044301 (2003).
 [2] M. Houssais and D. J. Jerolmack, “Toward a unifying constitutive relation for sediment transport across envi-

ronments,” *Geomorphology* **277**, 251–264 (2017).
 [3] R. Delannay, A. Valance, A. Mangeney, O. Roche, and P. Richard, “Granular and particle-laden flows: from laboratory experiments to field observations,” *Journal of Physics D: Applied Physics* **50**, 053001 (2017).
 [4] T. Börzsönyi, R. E. Ecke, and J. N. McElwaine, “Patterns in flowing sand: Understanding the physics of granular flow,” *Physical Review Letters* **103**, 178302 (2009).
 [5] A. J. Holyoake and J. N. McElwaine, “High-speed granular chute flows,” *Journal of Fluid Mechanics* **710**, 35–71 (2012).
 [6] N. Brodu, R. Delannay, A. Valance, and P. Richard, “New patterns in high-speed granular flows,” *Journal of Fluid Mechanics* **769**, 218–228 (2015).
 [7] GDR MiDi, “On dense granular flows,” *The European Physical Journal E* **14**, 341–365 (2004).
 [8] P. Jop, “Rheological properties of dense granular flows,” *Comptes Rendus Physique* **16**, 62–72 (2015).
 [9] V. Kumaran, “Kinetic theory for sheared granular flows,” *Comptes Rendus Physique* **16**, 51–61 (2015).
 [10] P. Jop, Y. Forterre, and O. Pouliquen, “A constitutive law for dense granular flows,” *Nature* **441**, 727–730 (2006).
 [11] K. Kamrin and G. Koval, “Nonlocal constitutive relation for steady granular flow,” *Physical Review Letters* **108**, 178301 (2012).
 [12] M. Bouzid, M. Trulsson, P. Claudin, E. Clément, and B. Andreotti, “Nonlocal rheology of granular flows across yield conditions,” *Physical Review Letters* **111**, 238301 (2013).
 [13] M. Bouzid, A. Izzet, M. Trulsson, E. Clément, P. Claudin, and B. Andreotti, “Non-local rheology in dense granular flows – Revisiting the concept of fluidity,” *The European Physics Journal E* **38**, 125 (2015).
 [14] Q. Zhang and K. Kamrin, “Microscopic description of the granular fluidity field in nonlocal flow modeling,” *Physical Review Letters* **118**, 058001 (2017).
 [15] É. Guazzelli and O. Pouliquen, “Rheology of dense granular suspensions,” *Journal of Fluid Mechanics* **852**, P1 (2018).
 [16] F. Boyer, É. Guazzelli, and O. Pouliquen, “Unifying suspension and granular rheology,” *Physical Review Letters* **107**, 188301 (2011).
 [17] M. Trulsson, B. Andreotti, and Philippe Claudin, “Transition from the viscous to inertial regime in dense suspensions,” *Physical Review Letters* **109**, 118305 (2012).
 [18] C. Ness and J. Sun, “Flow regime transitions in dense non-Brownian suspensions: Rheology, microstructural characterization, and constitutive modeling,” *Physical Review E* **91**, 012201 (2015).
 [19] C. Ness and J. Sun, “Shear thickening regimes of dense non-Brownian suspensions,” *Soft Matter* **12**, 914–924 (2016).
 [20] L. Amarsid, J.-Y. Delenne, P. Mutabaruka, Y. Monerie, F. Perales, and F. Radjai, “Viscoinertial regime of immersed granular flows,” *Physical Review E* **96**, 012901 (2017).
 [21] E. DeGiuli, G. Düring, E. Lerner, and M. Wyart, “Unified theory of inertial granular flows and non-brownian suspensions,” *Physical Review E* **91**, 062206 (2015).
 [22] M. Houssais, C. P. Ortiz, D. J. Durian, and D. J. Jerolmack, “Onset of sediment transport is a continuous transition driven by fluid shear and granular creep,” *Nature*

- Communications **6**, 6527 (2015).
- [23] M. Houssais, C. P. Ortiz, D. J. Durian, and D. J. Jerolmack, “Rheology of sediment transported by a laminar flow,” *Physical Review E* **94**, 062609 (2016).
- [24] R. Maurin, J. Chauchat, and P. Frey, “Dense granular flow rheology in turbulent bedload transport,” *Journal of Fluid Mechanics* **804**, 490–512 (2016).
- [25] V. Garzó, S. Tenneti, S. Subramaniam, and C. M. Hrenya, “Enskog kinetic theory for monodisperse gassolid flows,” *Journal of Fluid Mechanics* **712**, 129–168 (2012).
- [26] M. G. Chamorro, F. Vega Reyes, and V. Garzó, “Revisiting ignited-quenched transition and the non-newtonian rheology of a sheared dilute gas-solid suspension,” *Physical Review E* **92**, 052205 (2015).
- [27] S. Saha and M. Alam, “Revisiting ignited-quenched transition and the non-newtonian rheology of a sheared dilute gas-solid suspension,” *Journal of Fluid Mechanics* **833**, 206–246 (2017).
- [28] S. Chialvo and S. Sundaresan, “A modified kinetic theory for frictional granular flows in dense and dilute regimes,” *Physics of Fluids* **25**, 070603 (2013).
- [29] D. Vescovi, D. Berzi, P. Richard, and N. Brodu, “Plane shear flows of frictionless spheres: Kinetic theory and 3d soft-sphere discrete element method simulations,” *Physics of Fluids* **26**, 053305 (2014).
- [30] D. Berzi and D. Vescovi, “Different singularities in the functions of extended kinetic theory at the origin of the yield stress in granular flows,” *Physics of Fluids* **27**, 013302 (2015).
- [31] O. Durán, B. Andreotti, and P. Claudin, “Numerical simulation of turbulent sediment transport, from bed load to saltation,” *Physics of Fluids* **24**, 103306 (2012).
- [32] O. Durán, P. Claudin, and B. Andreotti, “Direct numerical simulations of aeolian sand ripples,” *Proceedings of the National Academy of Science* **111**, 15665–15668 (2014).
- [33] T. Pähz and O. Durán, “Fluid forces or impacts: What governs the entrainment of soil particles in sediment transport mediated by a Newtonian fluid?” *Physical Review Fluids* **2**, 074303 (2017).
- [34] T. Pähz and O. Durán, “The cessation threshold of non-suspended sediment transport across aeolian and fluvial environments,” *Journal of Geophysical Research: Earth Surface* **123**, 1638–1666 (2018).
- [35] T. Pähz and O. Durán, “Universal friction law at granular solid-gas transition explains scaling of sediment transport load with excess fluid shear stress,” *Physical Review Fluids* **3**, 104302 (2018).
- [36] M. Trulsson, E. DeGiuli, and M. Wyart, “Effect of friction on dense suspension flows of hard particles,” *Physical Review E* **95**, 012605 (2017).
- [37] A. Di Renzo and F. Di Maio, “Comparison of contact-force models for the simulation of collisions in DEM-based granular flow codes,” *Chemical Engineering Science* **59**, 525–541 (2004).
- [38] A. Di Renzo and F. Di Maio, “An improved integral non-linear model for the contact of particles in distinct element simulations,” *Chemical Engineering Science* **60**, 1303–1312 (2005).
- [39] R. Artoni and P. Richard, “Average balance equations, scale dependence, and energy cascade for granular materials,” *Physical Review E* **91**, 032202 (2015).
- [40] See Supplementary Material for nonlocal effects in gravity flows and sediment transport and for variance of c_μ with contact parameters.
- [41] C. Cassar, M. Nicolas, and O. Pouliquen, “Submarine granular flows down inclined planes,” *Physics of Fluids* **17**, 103301 (2005).
- [42] A. H. Clark, J. D. Thompson, M. D. Shattuck, N. T. Ouellette, and C. S. O’Hern, “Critical scaling near the yielding transition in granular media,” *Physical Review E* **97**, 062901 (2018).
- [43] N. Sela and I. Goldhirsch, “Hydrodynamic equations for rapid flows of smooth inelastic spheres, to burnett order,” *Journal of Fluid Mechanics* **361**, 41–74 (1998).
- [44] S. Saha and M. Alam, “Non-newtonian stress, collisional dissipation and heat flux in the shear flow of inelastic disks: a reduction via grad’s moment method,” *Journal of Fluid Mechanics* **757**, 251–296 (2014).
- [45] S. Saha and M. Alam, “Normal stress differences, their origin and constitutive relations for a sheared granular fluid,” *Journal of Fluid Mechanics* **795**, 549–580 (2016).
- [46] P.-P. Cortet, D. Bonamy, F. Daviaud, O. Dauchot, B. Dubrulle, and M. Renouf, “Relevance of visco-plastic theory in a multi-directional inhomogeneous granular flow,” *Europhysics Letters* **88**, 14001 (2009).
- [47] F. Legros, “The mobility of long-runout landslides,” *Engineering Geology* **63**, 301–331 (2002).
- [48] A. Lucas, A. Mangeney, and J. P. Ampuero, “Frictional velocity-weakening in landslides on earth and on other planetary bodies,” *Nature Communications* **5**, 3417 (2014).
- [49] B. C. Johnson, C. S. Campbell, and H. J. Melosh, “The reduction of friction in long runout landslides as an emergent phenomenon,” *Journal of Geophysical Research: Earth Surface* **121**, 881–889 (2016).